JOURNAL OF GEOPHYSICAL RESEARCH, VOL. 115, A01205, doi:10.1029/2009JA014423, 2010

Click Here for Full Article

On phase space density radial gradients of Earth's outer-belt electrons prior to sudden solar wind pressure enhancements: Results from distinctive events and a superposed epoch analysis

Drew L. Turner,[1,2] Xinlin Li,[1,2] Geoff D. Reeves,[3] and Howard J. Singer[4]

Received 1 May 2009; revised 30 July 2009; accepted 5 October 2009; published 14 January 2010.

[1] Here, we present the results of a study of phase space density radial gradients for outer-belt electrons at and beyond geosynchronous orbit prior to 86 sudden solar wind pressure enhancements from 1993 through 2007. All of the events are classified and analyzed based on the results for equatorial electrons with first adiabatic invariants of 50, 200, 750, and 2000 MeV/G. Examples of three distinctive events are compared, and the results from a superposed epoch analysis are presented. We find that the radial gradients are dependent on the first adiabatic invariant (i.e., energy), and that for the majority of cases, the gradient is negative for electrons with energies above a couple of hundred keV, while it is either positive or relatively flat for electrons with energies lower than this, which is evidence of two distinct populations. In the cases where a positive gradient is observed for 2000 MeV/G electrons, the solar wind and geomagnetic conditions are very quiet for at least two days prior to the event, but for the events when the gradient for the same electrons is negative, there is a consistent evidence of enhanced substorm activity and/or convection in the days leading up to the events. Overall, this study puts previous observations of phase space density (PSD) gradients into a broader context of solar wind and geomagnetic conditions, while encompassing a broad range of energies, from the source population of tens to hundreds of keV electrons to relativistic electrons with energies exceeding 1 MeV. We discuss how 41 of the 86 events are consistent with and can be explained by local heating by wave-particle interactions, and we provide evidence of the solar wind and geomagnetic conditions that are important to different types of sources of outer-belt electron PSD.

Citation: Turner, D. L., X. Li, G. D. Reeves, and H. J. Singer (2010), On phase space density radial gradients of Earth's outer-belt electrons prior to sudden solar wind pressure enhancements: Results from distinctive events and a superposed epoch analysis, *J. Geophys. Res.*, *115*, A01205, doi:10.1029/2009JA014423.

1. Introduction

1.1. Historical Context

[2] Despite five decades of research, the exact nature of the processes that control the Earth's outer radiation belt remains elusive. This region, which makes a torus-shaped "belt" around the Earth with inner and outer radial boundaries along the magnetic equator of around 3 R_E and 7 R_E, respectively, consists primarily of highly energetic electrons, the dynamics of which are affected by changes in the solar wind, magnetospheric field configurations, and other plasma populations. Many questions concerning the primary source and loss processes for these electrons remain unanswered. One such question, how electrons are accelerated to relativistic energies within the magnetosphere, was thought to be addressed with the inward radial diffusion theory presented in *Particle Diffusion in the Radiation Belts* [*Schulz and Lanzerotti*, 1974], but later spacecraft measurements and new analysis techniques implied that the radial diffusion theory alone could not account for electron acceleration in this complex region [e.g., *Reeves et al.*, 1998; *Li et al.*, 1999; *Brautigam and Albert*, 2000; also see discussions in review by *Friedel et al.*, 2002].

[3] The problem of electron acceleration has been reexamined within the past 15 years, and a new theory has arisen to explain the discrepancies between observations and the radial diffusion theory. *Temerin et al.* [1994] proposed a new mechanism in which plasma waves interact with the gyrating, trapped electrons, thus transferring energy to result in net electron acceleration. *Summers et al.* [1998] and

[1]LASP and Department of Aerospace Engineering Sciences, University of Colorado at Boulder, Boulder, Colorado, USA.
[2]Laboratory for Space Weather, Chinese Academy of Sciences, Beijing, China.
[3]Space and Atmospheric Sciences Group, Los Alamos National Laboratory, Los Alamos, New Mexico, USA.
[4]Space Weather Prediction Center, National Oceanic and Atmospheric Administration, Boulder, Colorado, USA.

Copyright 2010 by the American Geophysical Union.
0148-0227/10/2009JA014423$09.00

Horne and Thorne [1998] expanded upon this theory and identify whistler mode chorus waves as the energy donor for electrons with energies from hundreds of keV to several MeV. The theory of electron energization by wave-particle interactions has since been further examined and refined.

[4] At the heart of the acceleration question lie the electron phase space density (PSD) distributions. At any given time, the radial distribution of electron PSD for fixed values of the first and second adiabatic invariants (μ and K, respectively) is telltale of the acceleration mechanism responsible for electron energization [see discussion in *Green and Kivelson*, 2004]. Energization by inward radial diffusion requires the electron PSD for fixed μ and K to be higher at higher radial distances (referred to from now on as L^*, the Roederer L star parameter, which is related to the third adiabatic invariant and describes the radial distance in Earth radii to an electron's drift shell in the equatorial plane of Earth's magnetic field [see *Roederer*, 1970; *Selesnick and Blake*, 2000; *Green and Kivelson*, 2004]). In the other case, in situ acceleration by wave-particle interactions would result in a local peak in PSD around the L^* where the interactions are taking place. Thus, the radial gradient of outer-belt electron PSD can be used to imply the acceleration mechanism.

[5] Several previous studies have been conducted in attempts to identify the dominant mechanism using PSD radial gradients [i.e., *Selesnick et al.*, 1997; *Brautigam and Albert*, 2000; *Hilmer et al.*, 2000; *Selesnick and Blake*, 2000; *McAdams et al.*, 2001; *Green and Kivelson*, 2004; *Onsager et al.*, 2004; *Taylor et al.*, 2004; *Chen et al.*, 2005, 2006, 2007a, 2007b; *Iles et al.*, 2006; *Turner and Li*, 2008; *Tu et al.*, 2009]. Among these studies, *Hilmer et al.* [2000] used GPS dosimeter measurements and Los Alamos National Laboratory (LANL) flux measurements from geosynchronous orbit (GEO) to estimate the radial gradient of electrons with $\sim$90° pitch angles and μ = 2100 MeV/G during high-speed solar wind streams. They found that the gradient between GPS ($r \sim 4.2\ R_E$) and GEO ($r \sim 6.6$ RE) was positive (i.e., increasing with increasing radial distance) for 27 out of 31 cases studied. *Brautigam and Albert* [2000] found that for one storm, using CRRES data to calculate electron PSD for μ from 500 to 1000 MeV/G, the radial gradient was positive for smaller μ (<700 MeV/G) and negative for larger μ (>700 MeV/G), and they discussed several possible explanations for this, one of which is that an internal acceleration source existed for higher-energy electrons. *Selesnick and Blake* [2000] found evidence of PSD peaks between L of 4 and 6 from Polar data, and they discussed how PSD peaks can form either from local acceleration or from inward radial diffusion with a variable source at the outer boundary. They also discussed how PSD gradient calculations depend heavily on the magnetic field model used in the calculation. *Green and Kivelson* [2004] used data from the Polar spacecraft and the Tsyganenko models to calculate electron PSD gradients. They found that their results are best explained by acceleration from an internal source at $L \sim 5$, but the results are also strongly model-dependent. *Onsager et al.* [2004] calculated electron PSD gradients using two GOES measurements at different L^* around GEO (being at different magnetic latitudes, the GOES satellites are also located on different L^*). They limited their study to equatorially mirroring, $\sim$90° pitch angles, μ = 6000 MeV/G electrons, and their results indicate that the PSD radial gradient is positive for times of quiet geomagnetic conditions, meaning inward radial diffusion may be the primary energization mechanism under quiet conditions. Recently, *Chen et al.* [2007b] used Polar, LANL, and GPS satellite measurements to calculate the electron PSD at different radial distances. Their analysis covers two years, 2001–2002, and μ in the range 462–2083 MeV/G. They found frequent and sometimes persistent PSD peaks inside of GEO with no evidence of variations in the PSD at higher L^*, suggesting that local acceleration by wave-particle interactions is the primary acceleration mechanism for electrons in the outer belt.

1.2. Development and Application of a New Technique

[6] In the past, independent works by *Li et al.* [2003] and *Lee et al.* [2005] on particle injections resulting from interplanetary shocks found that the energetic (i.e., >225 keV) electron response can be an immediate decrease in the flux measured at GEO. *Li et al.* [2003] explained this as a result of weaker source population at larger radial distances for an event on 26 August 1998, and refer to previous test-particle simulation results, which show how particles are transported radially inward when the shock impacts the magnetosphere, as further evidence [i.e., *Li et al.*, 1993; *Li et al.*, 1998]. In *Lee et al.* [2005], they also found that for "compression-only" injections of high-energy electrons, there are often immediate dropouts in electron fluxes. They discussed that a decrease or little change in particle flux due to an injection from a dynamic pressure impulse is evidence that the particle distribution function (i.e., PSD) at constant first and second adiabatic invariants decreased or was approximately constant with increasing radial distance. *Shi et al.* [2009] conducted a more comprehensive study of the energetic flux response to 128 solar wind dynamic pressure enhancements from 2000 to 2003, and they found that the dominant response for relativistic electrons measured at GEO is a decrease in flux.

[7] Recently, *Turner and Li* [2008] introduced a new analysis technique to determine the direction of the PSD radial gradient at and beyond GEO, immediately prior to sharp solar wind pressure enhancements, referred to, throughout this paper, as pressure pulses. When the magnetosphere is impacted by a solar wind pressure pulse, the impulse in the dynamic pressure results in a magnetic field compression and the inward radial transport of trapped outer-belt electrons, which conserve their respective μ and K in the process [*Li et al.*, 1993, 2003; *Lee et al.*, 2005]. Thus, immediately after such a pressure pulse, magnetic field and electron flux measurements from GEO are used to determine the PSD at increasingly higher L^* (i.e., at a fixed location, L^* before the compression is less than L^* after the event). *Turner and Li* [2008] used flux data from the Los Alamos spacecraft in GEO to calculate electron PSD for a broad energy range, and they calculated μ for all energies by scaling the magnetic field measured by the nearest GOES satellite to the LANL satellite being used to get the PSD. From this, the PSD for near-equatorial electrons with fixed μ can be calculated before and after the pressure pulse to determine the sign of the PSD gradient beyond GEO. This process requires that specific criteria be met, which is discussed further in section 3. Two of the signif-

icant advantages of this new technique are that it does not rely on empirical magnetic field models for long periods of time or when the models become highly inaccurate (i.e., after the pressure pulse impact) and that it can be used to determine the direction of the PSD gradient nearly instantaneously using particle measurements from only a single spacecraft. *Turner and Li* [2008] found that the direction of the PSD gradient for ~1 MeV electrons at GEO prior to the events is negative for the majority of events examined. Also, they discussed how the PSD gradient is μ-dependent: the gradient for higher-μ electrons is often significantly different than that for lower-μ electrons.

[8] Here, we employ the method of *Turner and Li* [2008] to determine the direction of the PSD radial gradients of equatorially mirroring electrons over a wide range of μ at and beyond GEO prior to 86 solar wind pressure pulse events that occurred over more than one full solar cycle (1993–2007). We first discuss the data used to conduct this study and the criteria we use to determine our set of events. A case study of three individual events, each displaying a distinctive type of PSD result, follows. The results of a superposed epoch analysis are then presented prior to a comprehensive discussion of the results, which focus on the various solar wind and geomagnetic preconditions that lead to different types of PSD gradients beyond GEO, and their implications. We also discuss how these results provide important insight and context to the results from previous PSD gradient studies while expanding our understanding of not only the gradients for relativistic electrons, but those for the source population of tens to hundreds of keV electrons as well. Finally, conclusions are presented, followed by a discussion of potential future work.

2. Data Set Description

[9] This study requires various types of data from several different sources. Electron flux data from the synchronous orbit particle analyzer (SOPA) instruments on various LANL spacecraft in GEO have been obtained from the LANL online data request system (available at: http://leadbelly.lanl.gov/lanl_ep_data/). For this study, flux data at a 10 s resolution is used from the SOPA instruments' nine differential energy channels, which cover a full energy range from 50 keV to 1.5 MeV. These data are used to calculate the PSD during each event, as well as for the electron population characteristics in the superposed epoch analysis. GOES magnetic field measurements are used to determine event eligibility based on the study criteria (discussed in section 3), as well as to determine the field compression during each event. These data were obtained at a 1 min resolution from NASA's coordinated data analysis Web site (CDAWeb; available at: http://cdaweb.gsfc.nasa.gov/) [*McGuire et al.*, 2000].

[10] For the individual event studies and the superposed epoch analysis, we used data from the following sets: solar wind velocity; number density; B_x, B_y, and B_z from in-house ACE data sets (for 1998–2007); and IMP-8 and OMNI data sets, which are both available from CDAWeb (for 1993–1997) (see http://omniweb.gsfc.nasa.gov/); *AL*, *AU*, *AE*, *Dst*, and *Kp* geomagnetic index data sets from the World Data Center for Geomagnetism, Kyoto, Japan (*AL*, *AU*, *AE*, and *Dst* sets available at: http://swdcwww.kugi.kyoto-u.ac.jp/index.html) and from CDAWeb (*Kp*, courtesy of the National Geophysical Data Center). Solar wind data from ACE and OMNI (1995–1997) are available at 1 min resolution, while OMNI data for 1993–1994 are available only at hourly resolution. *AL*, *AU*, *AE*, and *Dst* are used at 1 h resolution, while 3 hourly *Kp* is used.

[11] Solar wind dynamic pressure is calculated directly from the velocity and number density data, approximating the proton to alpha ratio to be 4:1 (i.e., 80% protons and 20% alphas). GSE magnetic field measurements are converted to GSM using the Office National d'Etudes et de Recherche Aérospatiales (ONERA) Deployment Environmental Surveillance Program (DESP) library tools (http://craterre.onecert.fr/support/user_guide.html). Other parameters (e.g., magnetic field magnitude (B_{tot}), solar wind V-Bsouth (VB_s), plasmapause location (L_{pp}), and the Akasofu ε parameter) are also calculated from the appropriate data sets and were examined for this study, though not all of the parameters examined are presented here. Two additional parameters that we discuss throughout are AE^* and Dst_{min}, which are defined, respectively, at any particular time as the maximum value of the *AE* index from the previous 3 h and the minimum value of the *Dst* index from the previous 3 h.

3. Event Criteria

[12] As discussed by *Turner and Li* [2008], this study requires that we use only sudden pressure-enhancement events in which the solar wind pressure pulses occur on timescales significantly shorter than the electrons' drift periods (i.e., risetimes less than ~2 min). This requirement ensures that the spacecraft flux measurements after the pressure pulse impact are of electrons that were at approximately the same local time but a higher L^* prior to the pressure pulse. After identifying these types of pressure pulses in the solar wind data set, we further narrow the events down by the magnetic compression observed by the GOES spacecraft in GEO. We only use events in which there is a positive overall compression of the magnetic field that is also relatively uniform over different local times. To test the uniformity of the compressions, we compare the percent increase from two or more spacecraft, which are most often two GOES satellites separated by approximately 4 h in local time, and only use events in which the percent increases of the measured compressions differ by less than 25%. Finally, to qualify as a useable event, at least one LANL spacecraft must be on the dayside, between 0600 LT and 1800 LT, at the time of the pressure pulse impact.

[13] We have identified over 145 sudden pressure pulse events in which the solar wind dynamic pressure (from IMP-8, ACE, and OMNI data sets) increases by more than half of its original level in less than 2 min. After the geosynchronous magnetic field compression criteria are applied to this set, the number of useable pressure pulses is reduced to 86. Figure 1 shows how these events are distributed over the period from 1 January 1993 to 1 January 2008. In Figure 1, events are plotted on the *y* axis by their respective percent increase in solar wind dynamic pressure. Events that are used in this study are marked by the black asterisks, while other events that were identified but not used due to the event criteria are marked by the red crosses.

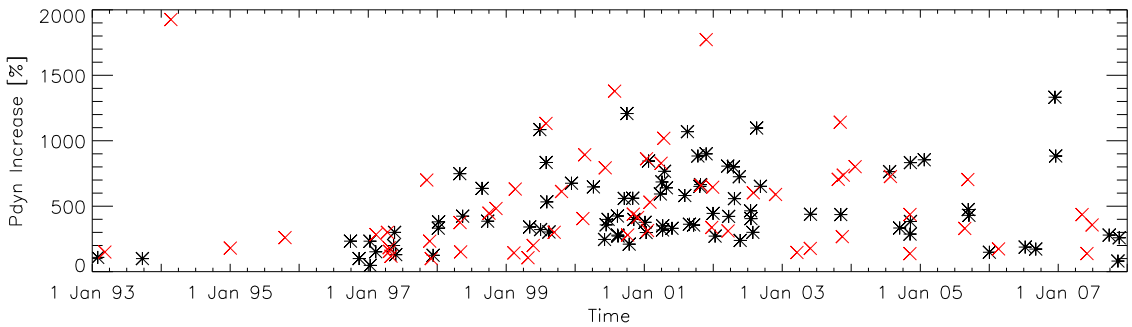

Figure 1. Event distribution in time from 1993 to 2007 and scaled by the pressure pulse percent increase. Pressure pulses that meet the event criteria are shown with black asterisks, while those that do not are shown with red crosses.

Notice how the events are mostly concentrated around solar maximum, with half of the events used in the study (43 of the 86) occurring between January 2000 and September 2002.

4. Study of Distinctive Events

[14] In this section, we discuss the characteristics of distinct types of events that we have identified through this analysis. We classify each type of event based on the behavior of the PSD for four fixed values of μ: μ = 50, 200, 750, and 2000 MeV/G, which correspond to electrons near dayside GEO with energies around 50 keV, 200 keV, 600 keV, and 1 MeV, respectively. Table 1 shows the number of events in which the PSD gradients for each of these four μ values are negative, flat, and positive. To be considered as a "negative gradient event," the PSD for some fixed μ after the event must drop to less than 90% of the PSD (for the same μ) averaged two-and-a-half minutes before the event, whereas to be classified a "positive gradient event," the PSD must increase to more than 110% of the before-event PSD average. Those events classified as "flat" fall in between these two other types. Note that for 75% of events, the PSD gradient for electrons with μ = 2000 MeV/G is negative, while the gradient for electrons with μ = 50 MeV/G is positive or flat for 72% of events. Meanwhile, the PSD gradient for electrons with μ = 200 MeV/G, which have energies near GEO of around a couple of hundred keV, are split almost evenly between negative and positive/flat events. These results are consistent with the results of *Chen et al.* [2007b] for relativistic electrons and with the initial findings of *Turner and Li* [2008], who discussed how the PSD gradient beyond GEO is μ-dependent and there is some transition from mostly positive or flat gradients to mostly negative gradients for electrons with energies near GEO around a couple of hundred keV.

[15] The majority of the events can be more generally classified based on their overall PSD gradient results into the following four categories: (1) the PSD gradients for all μ's examined are negative, (2) the PSD gradients for all μ's examined are positive, (3) the PSD gradients for all μ's examined are flat, and (4) the PSD gradients for high-energy electrons are different than those for lower-energy electrons. There are two exceptional cases, both of which exhibit evidence of a peak in the high-energy electron PSD gradients beyond GEO. However, these exceptional case results are somewhat ambiguous since the observed peaks may be the result of either a brief dip in the dynamic pressure during the compression or an actual peak in the PSD gradient. Table 2 lists how many events can be classified into each of these categories.

[16] Three example cases will be discussed in the following subsections. The first example exhibits several events, but we pay attention primarily to two of these: an event where all gradients are negative and an event where all gradients are flat. The second example exhibits an event where all gradients are positive, and the third is for a "mixed" event exhibiting a negative gradient for 2000 MeV/G electrons, but a positive gradient for 50 MeV/G electrons. Figure 2 shows the PSD results for four different μ's (50, 200, 750, and 2000 MeV/G) from the three events used to set the epoch times (ETs) in each of the examples. In Figure 2, each event is color- and symbol-coded, and time is given in epoch minutes for 3 min before and after the pressure pulse impact time, which is the time used to determine the PSD gradient to avoid ambiguities due to electron drift (discussed by *Turner and Li* [2008]).

[17] For each example, corresponding Figures 3–8 show several solar wind parameters (i.e., dynamic pressure P, total velocity V, interplanetary magnetic field (IMF) magnitude B, IMF B_z in GSM, and VB_s), geomagnetic indexes (i.e., Kp, AE, and Dst), LANL electron fluxes, and the

Table 1. Amount of Events in Which the Phase Space Density Gradient for Electrons With μ = 50, 200, 750, and 2000 MeV/G Are Negative, Flat, or Positive[a]

	Negative	Flat	Positive
50 MeV/G	24 (28%)	29 (34%)	33 (38%)
200 MeV/G	39 (45%)	28 (33%)	19 (22%)
750 MeV/G	50 (58%)	29 (34%)	7 (8%)
2000 MeV/G	65 (75%)	16 (19%)	5 (6%)

[a]Percentage of total (86 events) is displayed in parentheses.

Table 2. Amount of Events by Overall Gradient Category[a]

All-Negative Gradients	All-Positive Gradients	All-Flat Gradients	Mixed Gradients	Evidence of a Peak
23 (26.7%)	4 (4.7%)	9 (10.5%)	48 (55.8%)	2 (2.3%)

[a]Percentage of total (86 events) is displayed in parentheses.

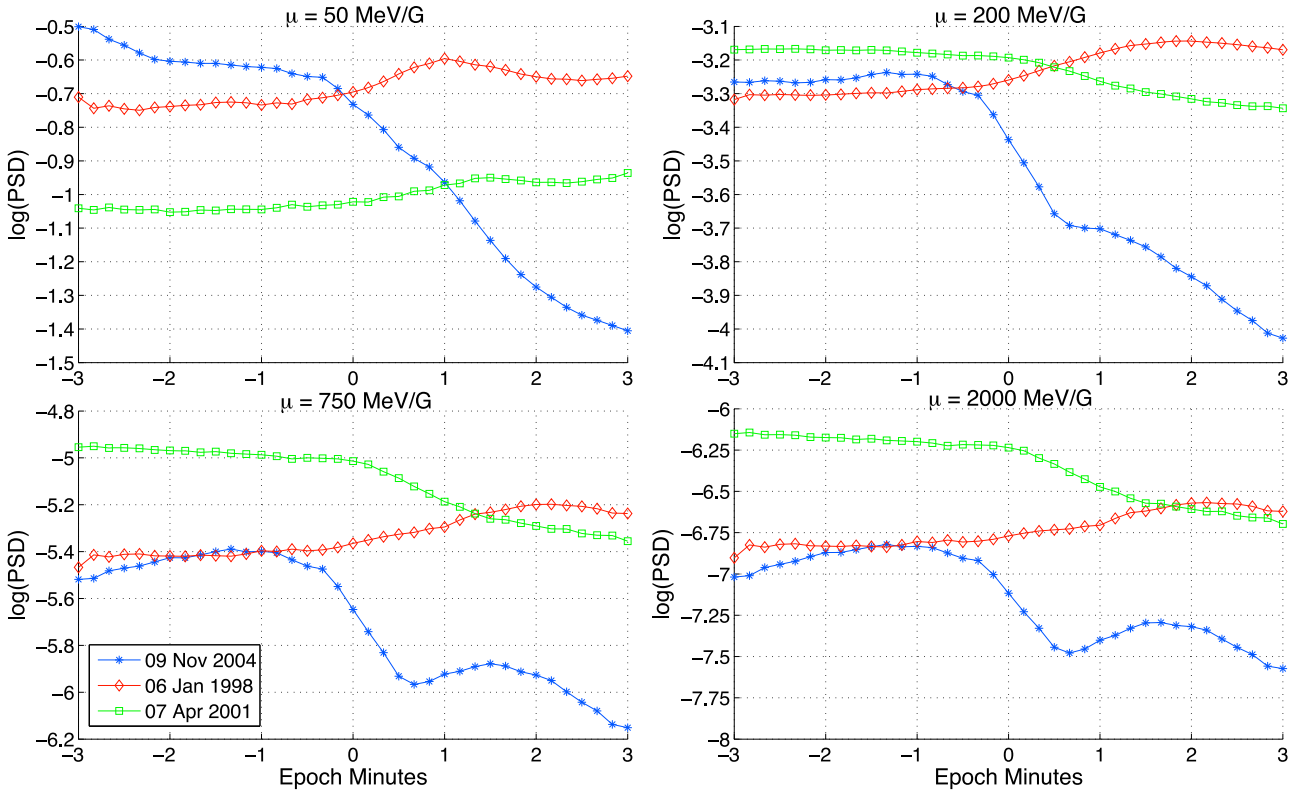

Figure 2. Phase space density (PSD) results (PSD units: c^3 MeV^{-3} cm^{-3}, where c is the speed of light) from three example events. Logarithm of phase space density is shown for four different values of μ: (top left) 50 MeV/G, (top right) 200 MeV/G, (bottom left) 750 MeV/G, and (bottom right) 2000 MeV/G. Events are color- and symbol-coded (see embedded legend).

derived PSD for different μ. For the solar wind and geomagnetic indexes plots, time is given in epoch hours, where the epoch is defined as the impact time. Note, however, that the ET is different for ACE and the magnetosphere (since the solar wind passes ACE at its L1 orbit shortly before it hits the magnetosphere), but they have been aligned throughout for Figures 3, 5, 7, and 9. The date and time at the top of Figures 3, 5, and 7 is the ET of the pressure pulse impacts with the magnetosphere. Figures 3, 5, and 7, comparing the different types of events, have the same range for each of the plotted parameters for comparison purposes. Also note, solar wind number density is not displayed since its characteristics are so similar to dynamic pressure. Figures 4, 6, and 8 show electron fluxes from four differential energy channels: 50–75 keV, 150–225 keV, 500–750 keV, and 1.1–1.5 MeV. For the first and third examples, the flux measurements that are used to calculate the PSD, which is, in turn, used to classify each event, are examined. For the second example, flux measurements from the spacecraft used to calculate the PSD have several large gaps in the days leading up to the event, so measurements from another spacecraft are displayed instead. For this study, we use 10 s resolution flux data, but for these event flux plots, we have smoothed the data for clarity. Time is given in epoch hours, where the ET is the time of the pressure pulse's impact with the magnetosphere, and is the same as that used in the solar wind and geomagnetic index plots. With the exception of the first example, ETs for these flux plots only go back to −48 h due to a combination of missing days in the data and results from the superposed epoch analysis that are discussed in the next section. Finally, the PSD results from each event are also shown individually in the same format as in Figure 2.

4.1. Example Event 1: All-Negative and All-Flat PSD Gradients

[18] The first example to be discussed is actually an interesting series of several different events. Figure 3 shows the solar wind parameters and geomagnetic indexes for this series of events. ET here is set to an event that is used in this study and reveals a decrease in PSD (i.e., negative gradients) over a full range of μ's immediately following the pressure pulse impact. For this event, the negative gradients, which result from a lack of source populations for electrons at all energies, are likely due to loss at higher L^*'s from the pressure pulse that occurs ~9 h before the ET, where the dynamic pressure spikes to more than 10 nPa and stays high up to the ET. The series of pressure pulses in the days leading up to this event present an interesting, though complex, scenario to this study. Two of the pressure pulses on 7 November (at −64 and −56 h ET) are not used for this study, since they do not meet the event criteria due to the lack of a large pressure enhancement in the first event, as well as inconsistencies in the associated magnetic field compressions measured by GOES 10 and GOES 12. However, looking only at the LANL data in Figure 4 (top), we can infer that prior to the second pressure pulse (first dash-dot vertical line from the left at about −56 h ET), the PSD

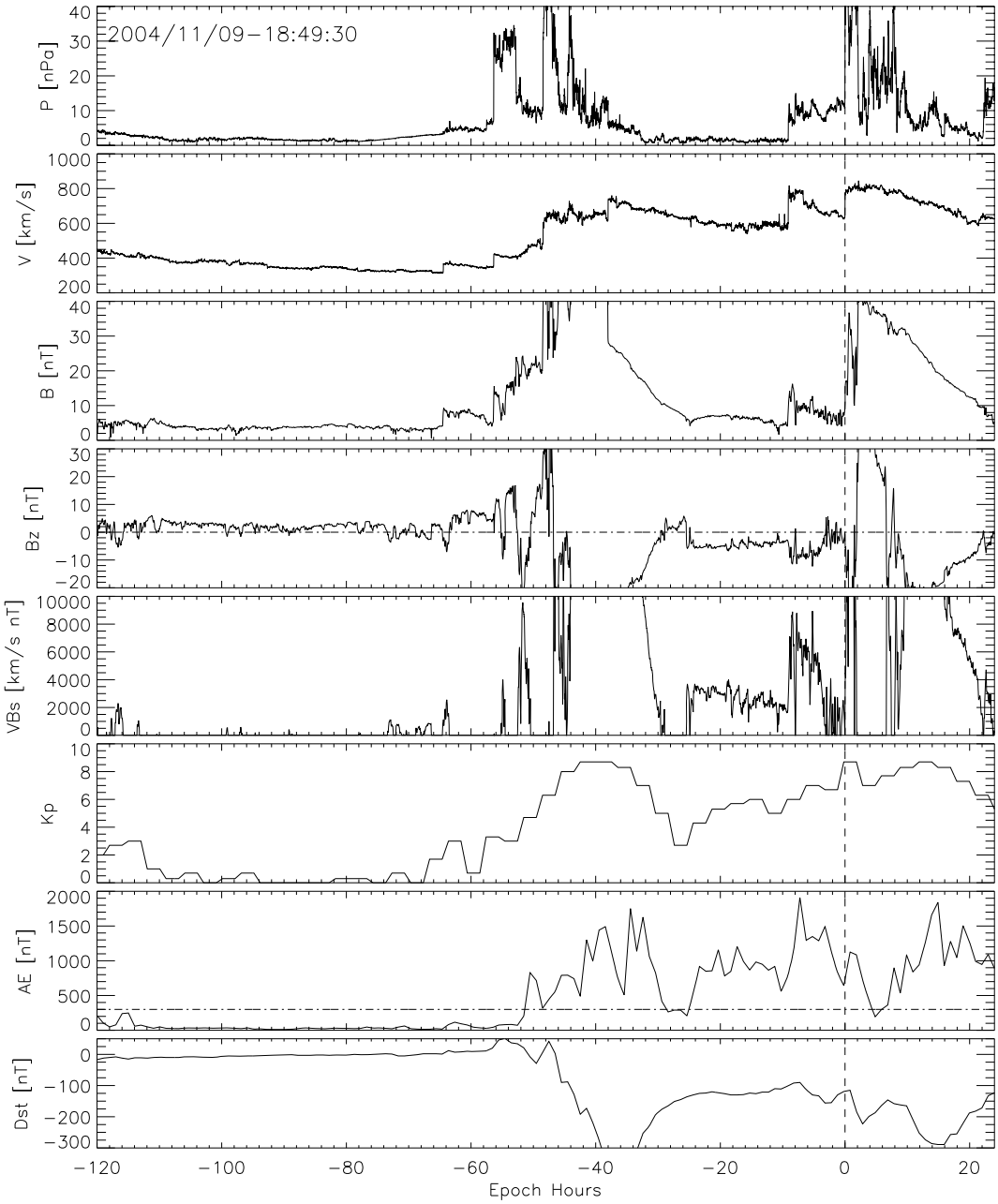

Figure 3. Solar wind and geomagnetic conditions for five days before and one day after an event on 9 November 2004. Epoch time is given in the top left.

gradient was negative for electrons with energies greater than a couple hundred of keV, since their fluxes either stay relatively the same or decrease significantly immediately after the pressure pulse impact. Also, the fluxes for lower-energy electrons increase immediately after this pressure pulse, but it is impossible to say what the direction of their PSD gradient was without more confidence in the magnitude of the magnetic field compression. This flux behavior is also the same for three LANL satellites on the dayside for this event. The third pressure pulse on 7 November (shortly before −48 h ET and marked with the second dash-dot line from the left in Figure 4) does meet all the criteria, and this pressure pulse reveals all negative PSD gradients, which is possibly due to enhanced magnetopause losses from the previous two events. Two days later, the pressure pulse at −9 h ET (third dash-dot line from left in Figure 4) results in flat PSD gradients for μ's of 2000, 750, and 200 MeV/G, and a positive PSD gradient for μ = 50 MeV/G. This is significant because it shows that in the two days between pressure pulses, the source populations at higher L^* have been replenished. Concerning this, notice the sudden flux increase at around −33 h ET, where the flux for all channels increases abruptly by more than an order of magnitude, and then stay at these new levels. These flux data are from LANL satellite 1991−080, which is at 07:49 LT at 0 h ET; therefore, at −33 h ET, 1991−080 was on the nightside at 22:49 LT. Here, the 500−750 keV and 1.1−1.5 MeV levels increase together with the 50−75 and 150−225 keV

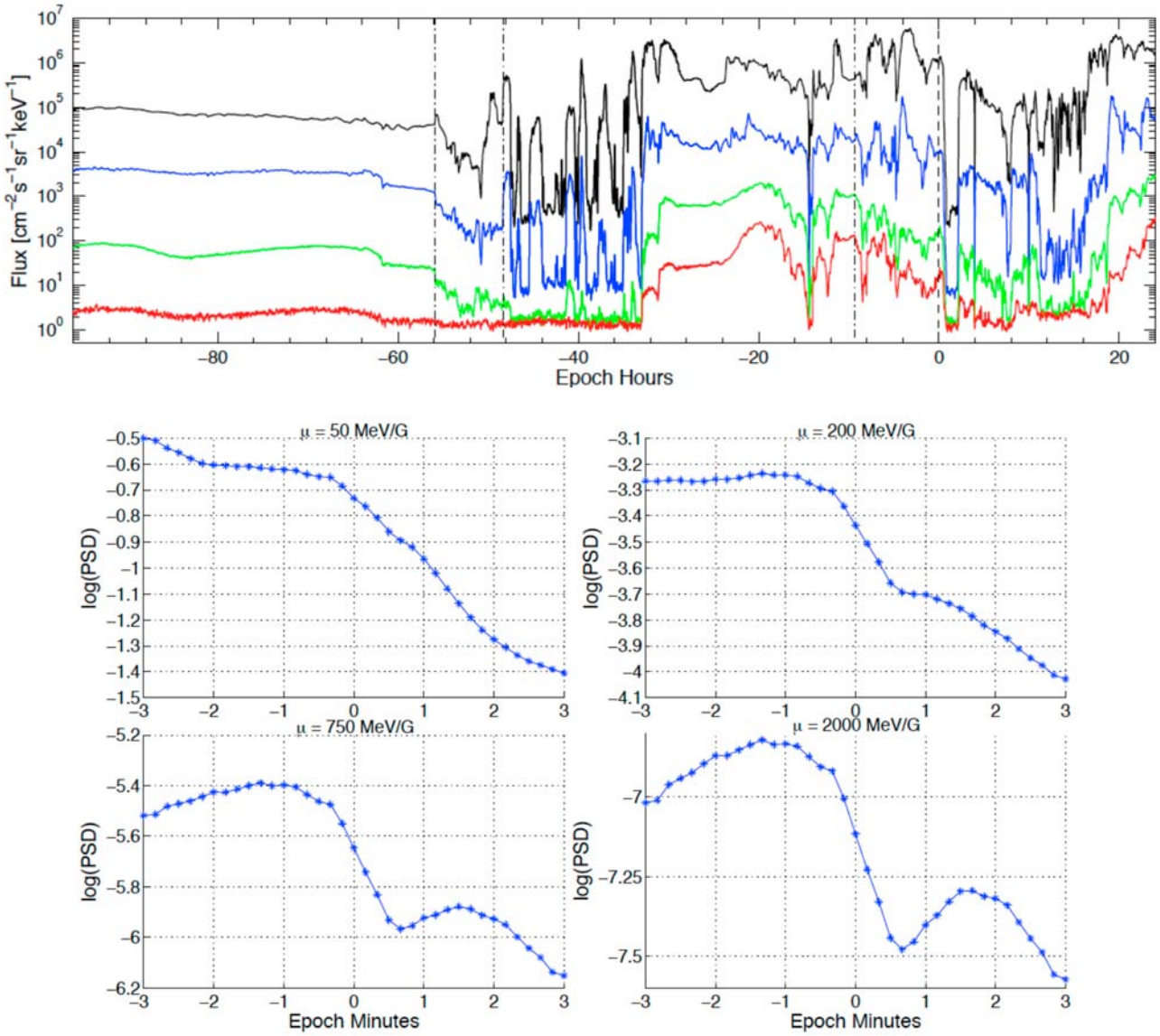

Figure 4. (top) Electron fluxes from LANL satellite 1991–080 for the 9 November 2004 event. Epoch time is the same as that for Figure 3. Fluxes are shown from four different energy channels: 50–75 keV (black), 150–225 keV (blue), 500–750 keV (green), 1.1–1.5 MeV (red). For further details, see discussion in text. (bottom) Phase space density results from this event shown in the same format as Figure 2.

channels, but for the large fluctuations seen in the lower channels before this time, which are probably associated with enhanced substorm activity evident from the very high *AE* index levels, there are only small, similar variations in the 500–750 keV flux and absolutely no similar variations in the 1.1–1.5 MeV flux. This increase is likely due to a couple of substorm injections of both lower energy and relativistic electrons similar to the event discussed in *Ingraham et al.* [2001], who find that prolonged substorm activity during the recovery phase of the large storm that occurred on 24 March 1991 resulted in substorm injections of two different electron populations: one with energies ranging from 50 to 300 keV that are commonly injected by substorms and the other with energies from 0.3 to several MeV, to GEO within a few hours of local midnight. Similar to the 1991 event, at −33 h ET in Figures 3 and 4, 1991–080 is near ∼23:00 LT in GEO during the recovery phase of a large storm and a prolonged period of high substorm activity, when it observes a sudden injection of electrons over a broad range in energy from tens of keV to greater than 1 MeV. This injection likely explains how the source population at higher L^* is replaced prior to the all-flat gradients event that occurred one day later at around −9 h ET.

[19] It should be noted here that very different preconditions seem to be able to result in all-flat PSD gradients. In contrast to the example discussed previously, many of the all-flat gradient events have very calm solar wind and geomagnetic conditions in the days leading up to the event times. Part of this may be from event misclassification if the PSD after the pressure pulse does not change by at least 10% of the prepressure pulse average. However, nearly flat gradients imply that radial diffusion, either inward or

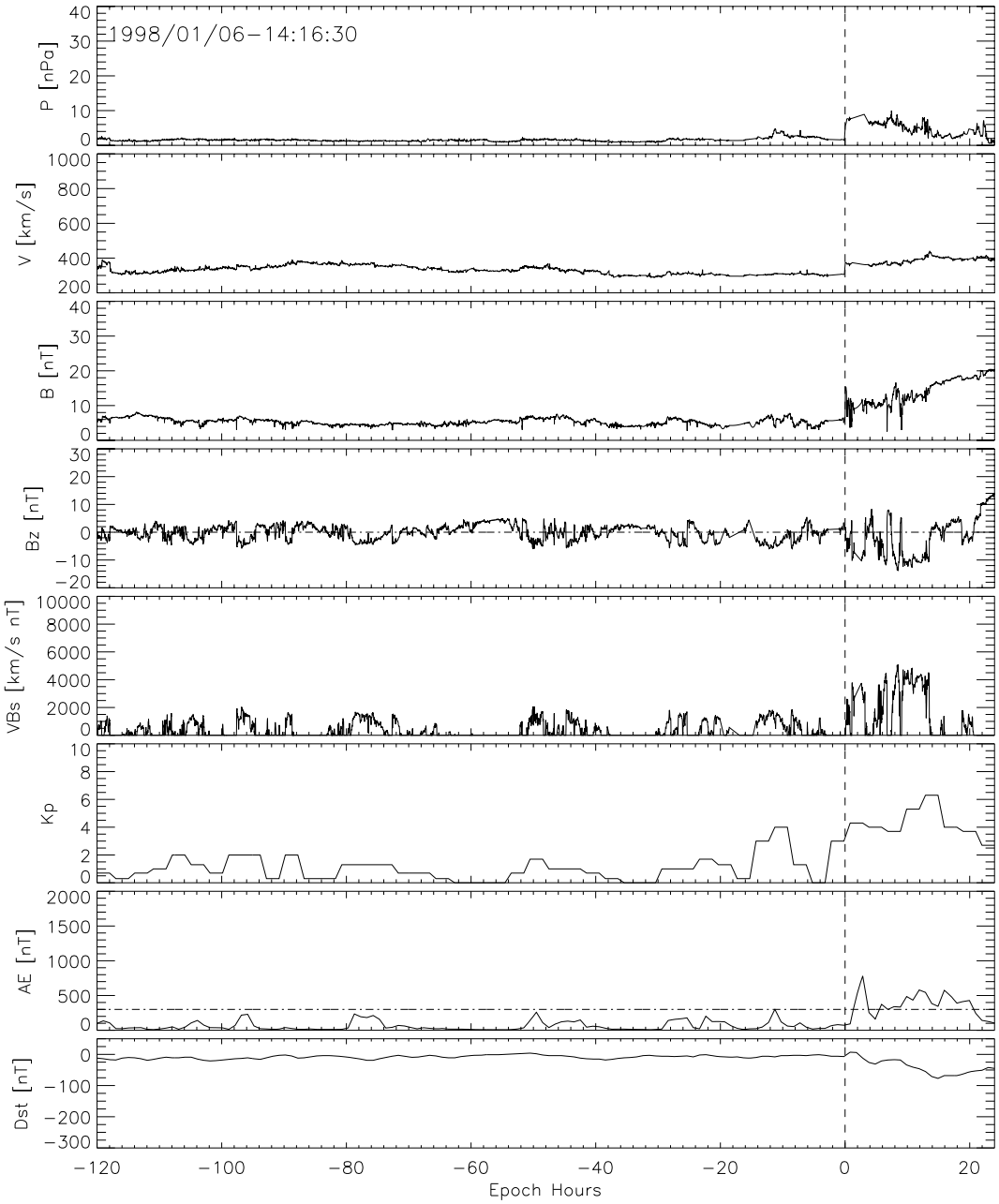

Figure 5. Solar wind and geomagnetic conditions for five days before and one day after an event on 6 January 1998. Epoch time is given in the top left.

outward, has smoothed the radial gradient and that radial diffusion will not be significant at and beyond GEO.

4.2. Example Event 2: All-Positive PSD Gradients

[20] As can be seen from Figure 6 (bottom), the PSD for all four μ's increases for this example, an event that occurred on 6 January 1998. This type of event, in which the gradients for the full range of μ's is positive, is one of the more uncommon types, with only 4 of the 86 events examined being classified as such (see Table 2 for numbers of each type of event). From Figure 5, we see that the solar wind conditions in the days leading up to the event are very calm, with no large enhancements in dynamic pressure, below-average velocity, low magnetic field magnitude, and only a few significant periods of southward IMF. This lack of activity is also apparent in the magnetosphere from the geomagnetic index data. The flux data in Figure 6 reflect these calm conditions, particularly in the 1.1–1.5 MeV channel (red). Figure 6 shows the fluxes measured by LANL-97A because the flux from 1990 to 095, which was at ~11:45 LT at the pressure pulse impact time and is used to calculate the PSD for this event, has several large data gaps in the days leading up to the event. Thus, fluxes from LANL-97A, at ~18:55 LT at the pressure pulse impact time, are shown to better illustrate the flux preconditions. From this, note that the lower-energy fluxes see particle injections at around −11 and −21 h, which correspond nicely with the minor *AE* activity around those same times

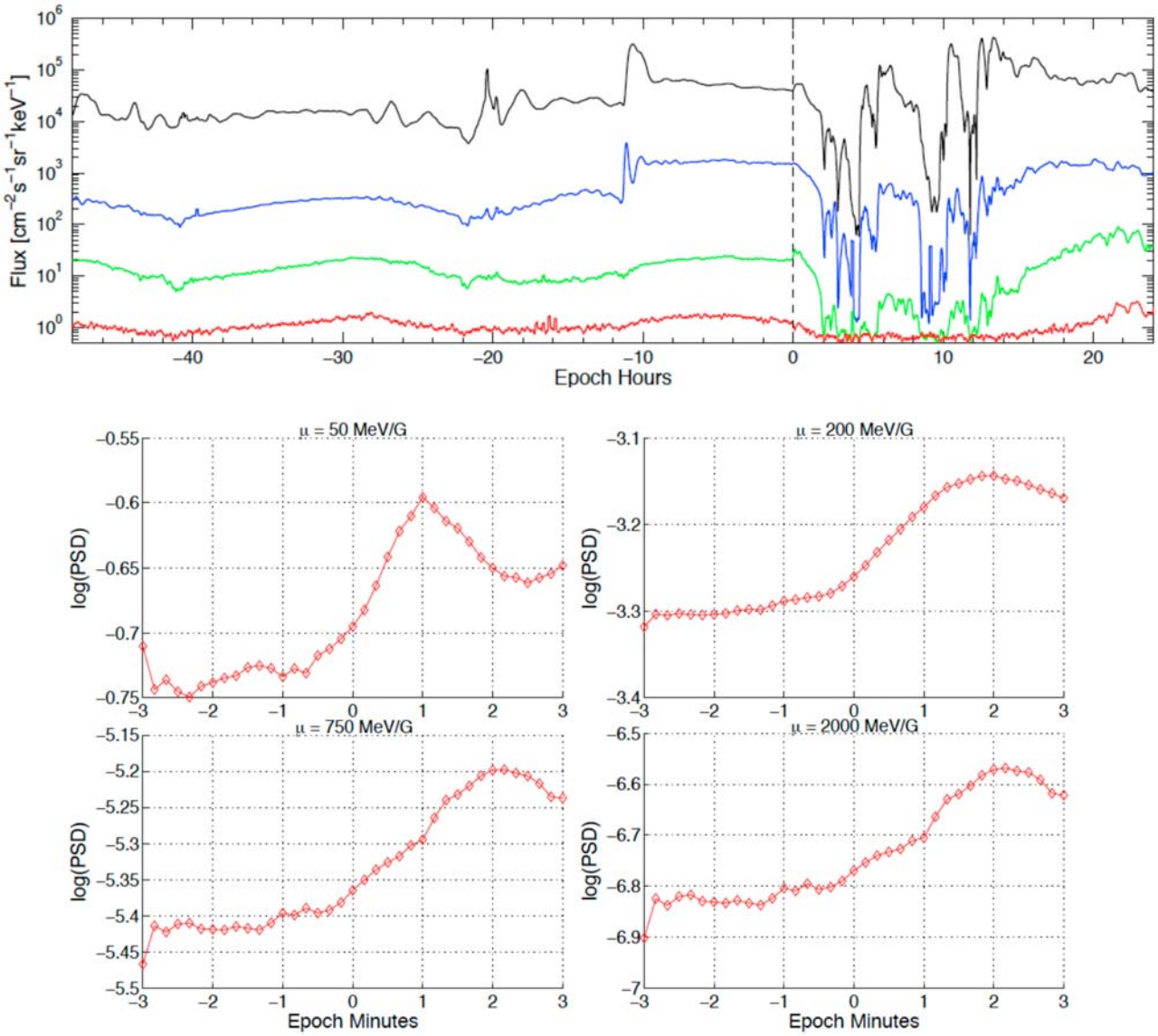

Figure 6. (top) Electron fluxes from LANL-97A for the 6 January 1998 event. Epoch time is the same as that for Figure 5. Colors correspond to the same four energy channels as in Figure 4. (bottom) Phase space density results from this event shown in same format as Figure 2.

and are probably substorm injections, but the higher-energy flux is quite constant other than the normal, diurnal variation. This quiet time and positive gradient scenario is consistent with the results of *Onsager et al.* [2004], who found that during a several-day period of low solar wind and magnetospheric activity in February 1996, the PSD gradient around GEO was positive.

[21] It is of interest here to briefly discuss how the PSD results can differ when using fluxes from different LANL spacecraft, which are at different local times around GEO, to derive the results. For this event, using fluxes from the spacecraft closest to noon (1990–095), which is how events are classified in this paper, the results are classified as an all-positive gradients event. However, when the same analysis is performed using fluxes from LANL-97A, the results are different; the PSD over the full range of μ remains relatively flat. This local time difference is potentially significant; it may result either because the two spacecraft are at different L^* or because LANL-97A was on the nightside and particles are not necessarily transported radially inward there. For further discussion on these local time differences, refer to *Lee et al.* [2005] and *Shi et al.* [2009], where the flux responses to sudden solar wind pressure pulses as measured by multiple LANL spacecraft are examined.

4.3. Example Event 3: Mixed PSD Gradients

[22] Figures 7 and 8 show the conditions for the most common type of event, in which there is a difference in the PSD gradients when those for electrons with μ of 50 MeV/G are compared to those for electrons with μ of 2000 MeV/G. Of this type of event, there are 23 cases where the PSD gradient is negative for 2000 MeV/G electrons but positive for 50 MeV/G electrons, 18 cases where it is negative for 2000 MeV/G electrons but flat for 50 MeV/G electrons, and 7 cases where it is flat for 2000 MeV/G electrons but positive for 50 MeV/G electrons. There are no cases where

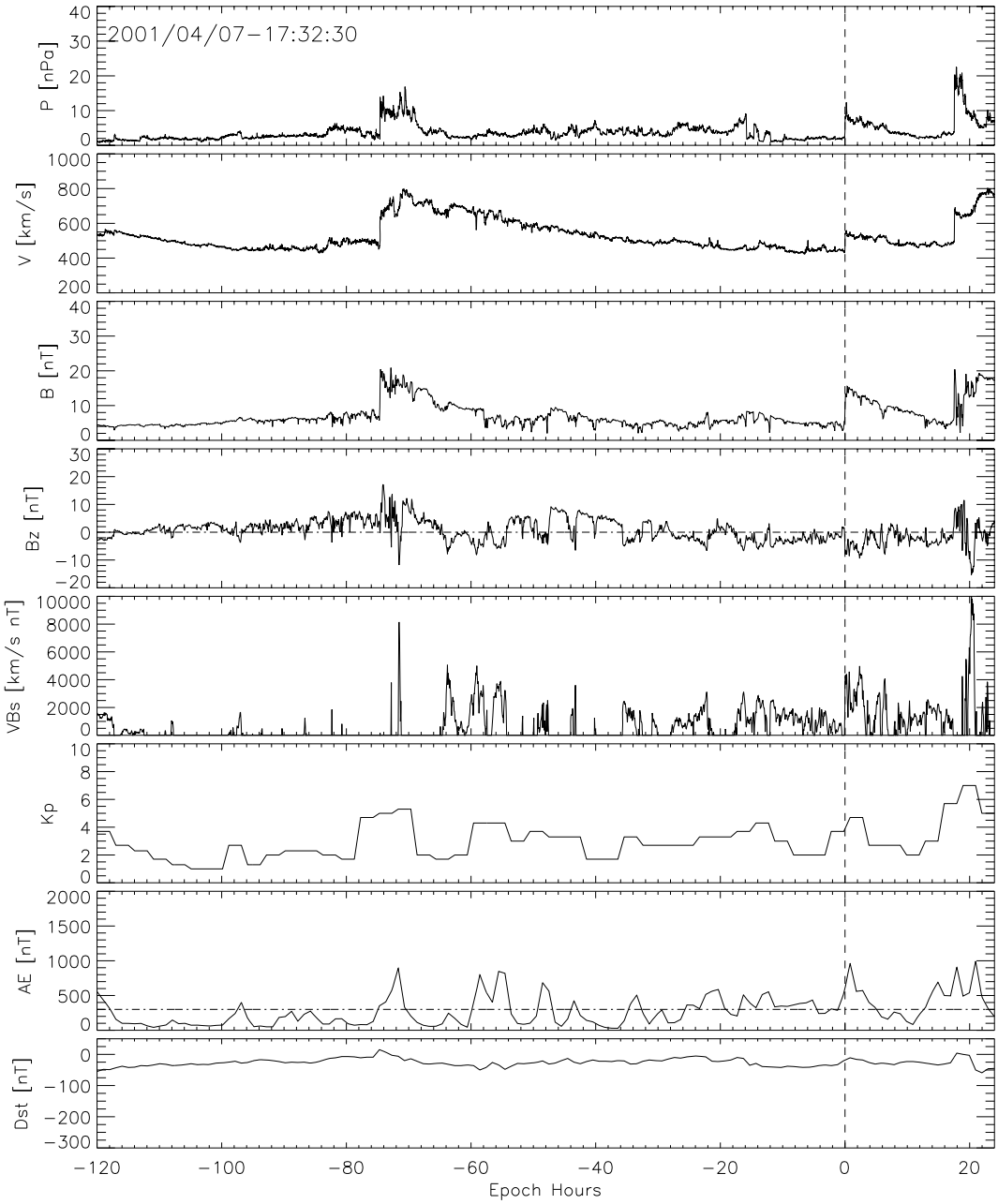

Figure 7. Solar wind and geomagnetic conditions for five days before and one day after an event on 7 April 2001. Epoch time is given in the top left.

the gradient is negative or flat for 50 MeV/G electrons but positive for 2000 MeV/G electrons.

[23] From Figure 7, one can see that there were three sudden pressure pulse events during the six days of time displayed. The first event, shortly after −75 h ET, is used in this study and classified as an all-negative gradients event. This event spawns some nearly continuous activity in the magnetosphere, which is evident in the *Kp* and *AE* indexes, but no large storm prior to the second pressure pulse at 0 h ET. This pressure pulse, occurring at 17:32 UT on 7 April 2001, is a mixed gradient event, where the PSD for electrons with μ = 50 MeV/G increases, while the PSD for μ's higher than 200 MeV/G all decrease, which is evident in Figure 8 (bottom). This implies that the PSD radial gradient was positive for lower-energy electrons and negative for electrons with energies greater than a couple hundred keV prior to the event. This is evidence of two distinct populations. A potential explanation of this case is that an internal heating source, potentially whistler mode chorus and/or magnetosonic waves generated by substorm-injected electrons and ring current particles, respectively, was active somewhere inside of GEO for electrons with energy greater than a couple hundred keV in the 0–3 days leading up to the event. Meanwhile, the positive gradients observed for lower-energy electrons are explained by a source population at higher L^*, most likely plasma sheet electrons injected during substorms. From Figure 8 (top), it is evident that in the days leading up to the event, the electron sources dominated

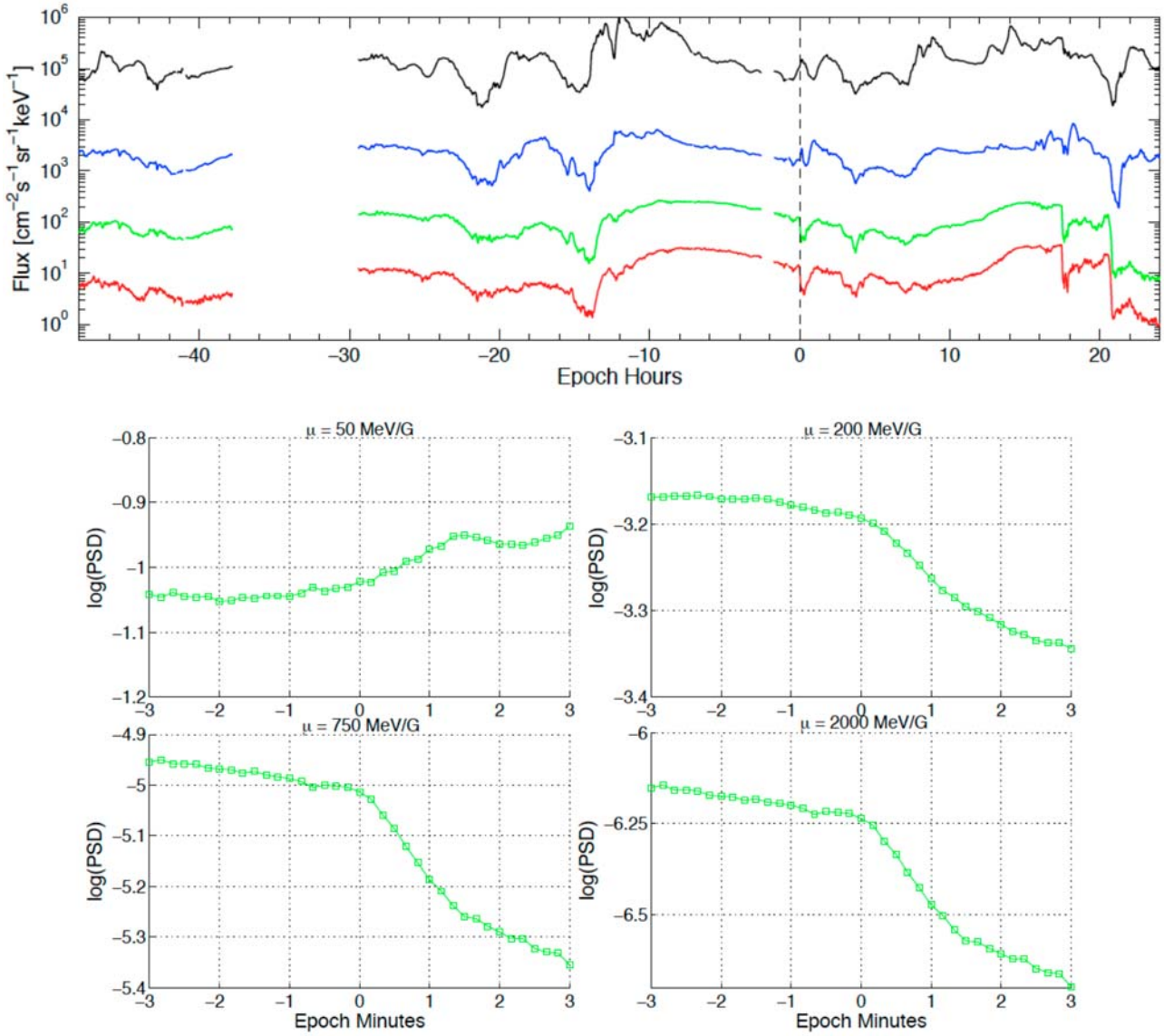

Figure 8. (top) Electron fluxes from LANL-01A for the 7 April 2001 event. Epoch time is the same as that for Figure 7. Colors correspond to the same four energy channels as in Figure 4. (bottom) Phase space density results from this event shown in same format as Figure 2.

slightly over electron loss, since the flux for all four energy channels increases overall prior to the event. Finally, the third pressure pulse, which occurs at around 17.5 h ET, is also used in this study and is classified as an all-negative gradients event in which the PSD for the full-range of μ's decreases most likely due to enhanced loss to the magnetopause from the pressure pulse at 0 h ET.

5. Superposed Epoch Analysis

[24] A superposed epoch analysis has been conducted to determine if there are any distinguishing characteristics in the statistical preconditions leading up to different types of events. We have gone through several different variations of this study, comparing different combinations of event types to one another, though here, we only discuss the results from one of these variations. For this analysis, all events are aligned by ET, which is once again defined as the pressure pulse impact times, and events are grouped to form two sets based on their type or PSD behavior for a particular μ. We compare 20 parameters in all, ten from the solar wind (dynamic pressure; total velocity; IMF magnitude; IMF B_x, B_y, and B_z in GSM coordinates; number density; VB_s; clock angle; and the Akasofu ε parameter), nine from geomagnetic index data (*Dst*, $Dst_{\min}$, *AU*, *AL*, *AE*, *AE**, *Kp*, and plasmapause locations derived from *Dst* [*O'Brien and Moldwin*, 2003] and *Kp* [*Carpenter and Anderson*, 1992]), and LANL electron fluxes. We compare the upper and lower quartiles, medians, and means of each parameter from the two sets of events for 120 h before the ET and 24 h after it for the solar wind and geomagnetic parameters, and 48 h before the ET and 24 h after it for electron fluxes. The two events from 1996 are not included in the epoch analysis since there are no *AE* data available from that year.

[25] The variation discussed here separates events into two groups based upon the sign of the gradient for electrons

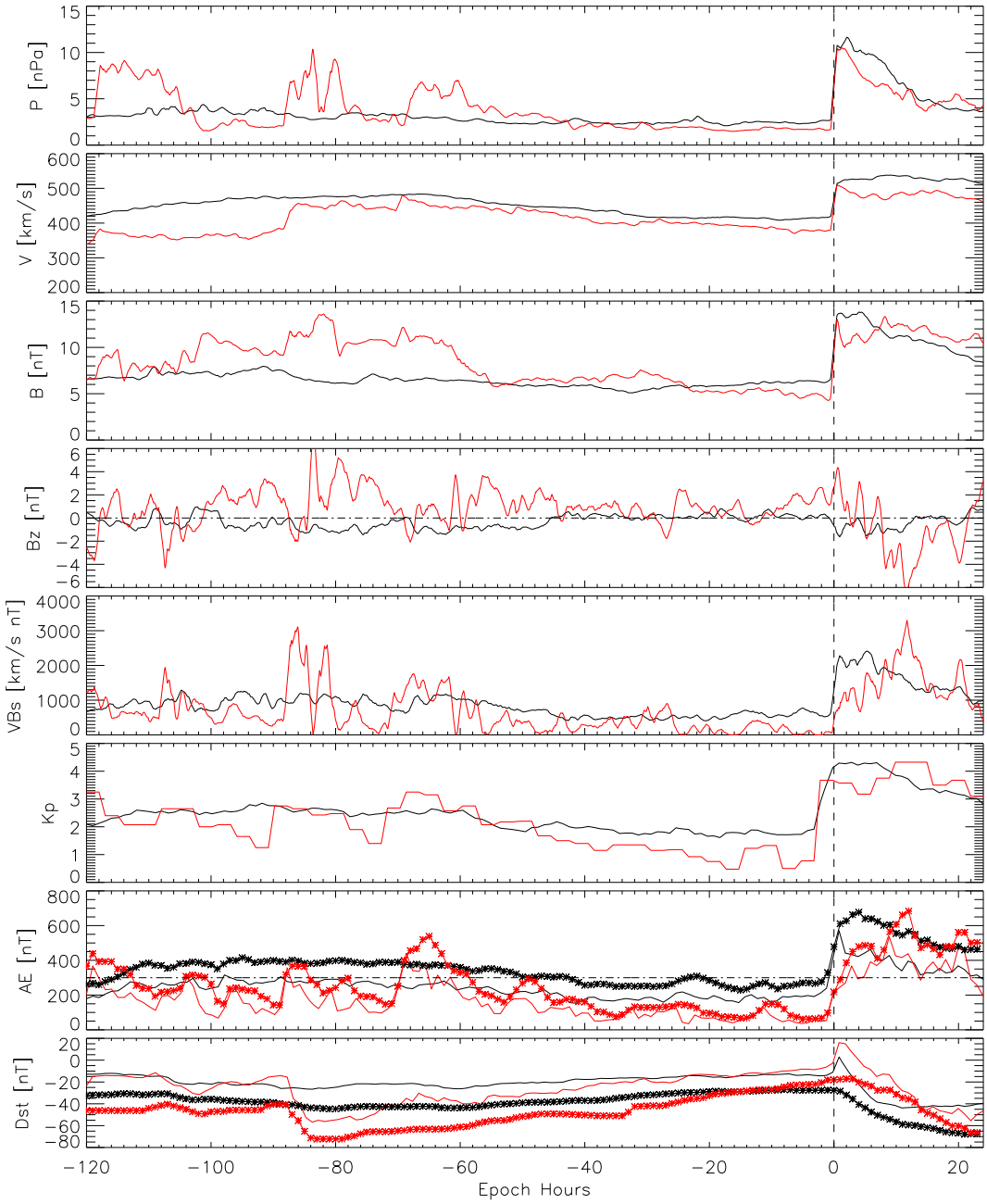

Figure 9. Solar wind and geomagnetic results from a superposed epoch analysis. Black curves represent the means from 2000 MeV/G negative gradient events, and red curves represent the means from 2000 MeV/G positive gradient events. For the *AE* and *Dst* plots, asterisks are used for *AE** and $Dst_{\min}$ means.

with μ = 2000 MeV/G: all those events in which a negative gradient is observed are grouped together to make one set, and all events in which a positive gradient is observed are grouped to make the second. The negative gradients set consists of 51 events since the all-negative gradient events in which loss to the magnetopause is suspected to be based on estimated magnetopause locations [*Petrinec and Russell*, 1996] in the days leading up to the event are not included. These are omitted because we understand, at least in part, why the gradients are all negative and also because they all have large events occurring in the days leading up to the actual event, which will skew the results. All-flat gradient events are not included since a wide range of preconditions can result in all-flat PSD gradients, which was discussed at the end of section 4.1. Results from this variation are shown in Figure 9. Means of each set are displayed and differentiated by color, with black curves corresponding to the negative gradients set and red curves corresponding to the positive gradients set. Here, we only show means, since quartiles for the positive gradients set are insufficient because there are only four of these events. Other pressure enhancement events are evident in the positive gradients data at around −118, −88, −82, and −69 h ET, and the evidence of these events is also present in the geomagnetic activity indexes, as can be seen in the *AE** enhancements and geomagnetic storm evident from the *Dst* curves. This

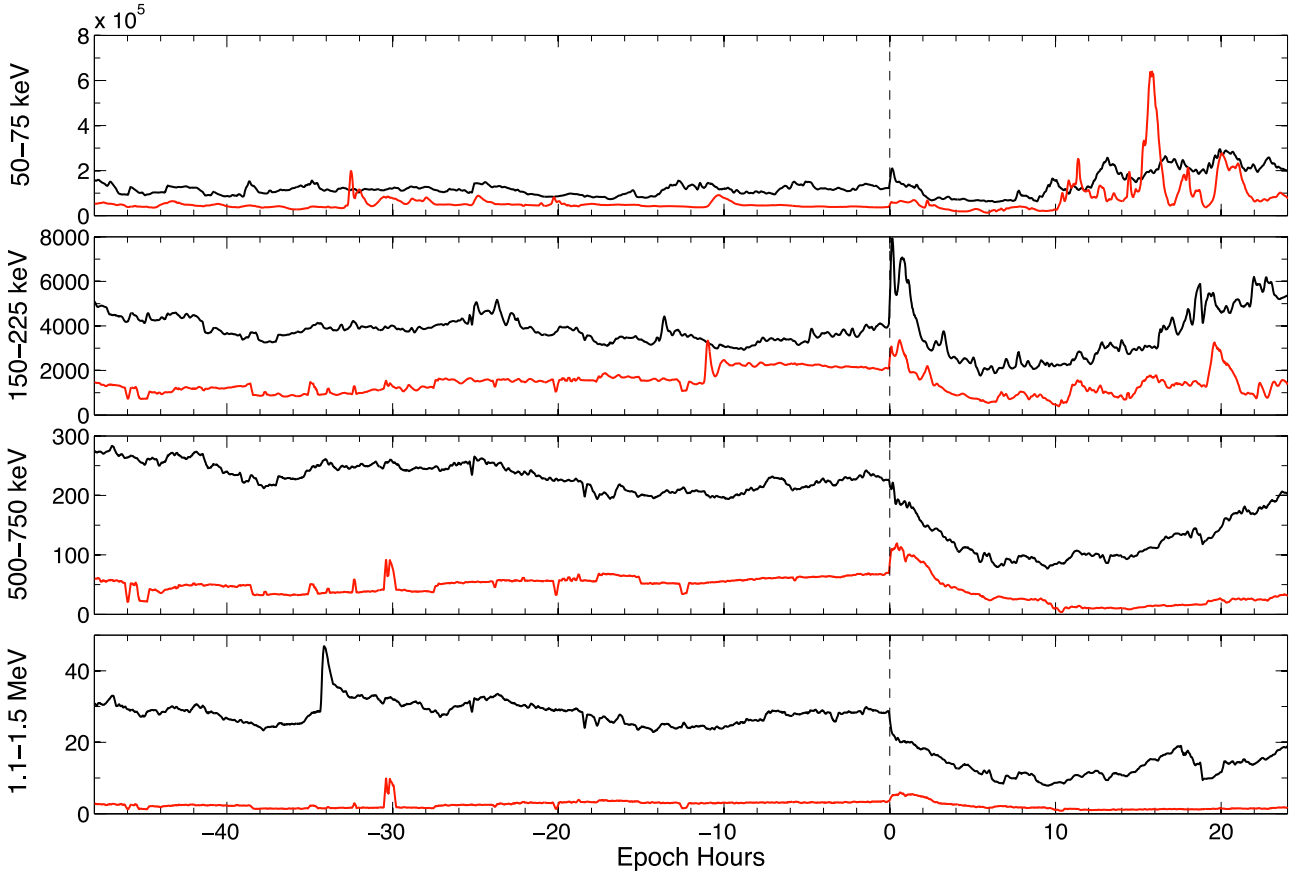

Figure 10. Electron flux results from a superposed epoch analysis. Results from four different energy channels are shown: 50–75 keV, 150–225 keV, 500–750 keV, and 1.1–1.5 MeV. Black and red curves correspond to mean fluxes from the same events used for the results in Figure 9.

activity is interesting, however, since only two of the four events see pressure enhancements and activity 3–5 days prior to the ET, and both of these are followed by at least two days of very calm conditions that stay calm right up to the ETs. The other two positive gradient events exhibit very calm conditions for more than five days prior to the ETs, as is shown in the second example case. In this same two days of time leading up to the negative gradient events, notice how the means of *Kp*, *AE*, and *AE** all stay relatively high compared to the positive gradient events. Also, notice that the mean B_z is almost entirely southward from around −98 to −44 h ET for the negative gradient events, while it is most often northward for the five days leading up to the positive gradient events. From Figure 10, it is clear that the average fluxes for the full range of LANL energies, 50 keV–1.5 MeV, are significantly higher prior to the negative gradient events than they are prior to the positive gradient events, and the difference between the two sets increases with increasing energy.

6. Discussion of Results

6.1. Basic Scenario

[26] The events discussed here can all be described using one basic scenario, in which radial diffusion redistributes outer-belt electron PSD from regions of high PSD to regions of lower PSD. In the radial direction, this redistribution is dependent on the radial gradient of the PSD between the two "sink" regions, the slot region between the inner and outer belts, and the magnetopause. We know some source of PSD is active because if it was not, then the outer belt would be empty due to the PSD diffusing to these two sinks. There are three potential sources of PSD for electrons near GEO: (1) radial transport from regions of higher PSD *inside* of GEO, (2) radial transport from regions of higher PSD *outside* of GEO, and (3) local acceleration of lower-energy electrons to higher energies near GEO. The effects from each of these source processes at GEO can be dependent upon electron energy, and the temporal history of the sources and sinks.

[27] With this basic scenario in mind, we can now discuss the various combinations of sources and sinks that can lead to the types of gradients that we observe in this study beyond GEO. Negative gradients beyond GEO can be the result of: (1) PSD outside the trapping boundary (e.g., in the plasma sheet) decreasing over time, (2) an earlier event increased the PSD inside of GEO and the electrons are still diffusing outward, (3) ongoing heating/acceleration of electrons inside of GEO, or (4) the PSD source not changing but an increased rate of diffusion at higher L^*. Positive gradients beyond GEO can be the result of the exact opposite situations occurring, i.e.: (1) PSD outside the trapping boundary *increasing* over time, (2) an earlier event *decreased* the PSD

inside of GEO and electrons are still diffusing *inward*, (3) ongoing heating/acceleration occurring *outside* of GEO, and (4) the PSD source not changing but a *decreased* rate of diffusion at higher L^*. Flat gradients observed in this study can result from diffusion smoothing out any PSD gradients beyond GEO or because the gradient was not sharp enough to classify as either positive or negative. A mix of PSD gradients for different μ's can occur when the source and sink processes are different for different energies. Finally, a peak in the PSD gradient beyond GEO can occur if: (1) the PSD gradient is originally positive, then there is some loss at higher L^*, (2) there is an "on-off" source at higher L^*, or (3) there is local heating/acceleration beyond GEO. For discussions on scenarios resulting in PSD peaks, see *Green and Kivelson,* [2004] and *Chen et al.* [2007b].

6.2. Discussion of the Example Cases

[28] We now offer some speculation as to which of the aforementioned conditions may have resulted in some of the events discussed in this study. The events in which the PSD over the full range of μ's examined is negative can be the result of any of the four source/sink conditions for negative gradients. However, for 12 of these events (out of 23 total), including the event in the first example, we can say with some confidence that the negative gradients are at least partially the result of enhanced losses to the magnetopause in the days leading up to the events. For the remaining 11 events, since the magnetopause does not come inside the range from which we expect the electrons to be transported inward during the field compressions (based on previous test-particle simulations by *Li et al.* [2003]), we can speculate that an internal source, an increased rate of diffusion at high L^*, or a decrease in the plasma sheet PSD is likely the cause of the negative gradients observed.

[29] Despite understanding the likely reason behind the all-negative gradients observed in the first example event, the series of events that occurred in the days leading up to this event introduced a very interesting case study. The intriguing thing about these events, which occurred between 7 and 9 November 2004, is that in the time span of just 39 h between the pressure pulse shortly before −48 h ET (in Figure 3) and the pressure pulse at −9 h ET, the source populations for both low-energy (50–200 keV) and high-energy (200 keV to >1 MeV) electrons is replenished. This timescale of around 1–2 days is important and will be repeated throughout this discussion of results. Also note that this replenishing of the source occurs during the recovery phase of a very large storm (see *Dst* data in Figure 3) in which there is significantly enhanced substorm and magnetospheric activity (see *AE* and *Kp* data in Figure 3) that result in substorm injections of electrons over an abnormally large energy range (tens of keV to >1 MeV; starting at around −33 h ET in Figure 4).

[30] The all-positive gradient events can be the result of any of the four aforementioned source/sink conditions for positive gradients, and thus, it is difficult to speculate the reason why these gradients are observed. PSD in the plasma sheet may have increased prior to these events, or losses at lower L due to an expanding plasmasphere (in more than 2 days of quiet conditions prior to these events) can decrease the PSD inside of GEO. Heating outside of GEO is possible, though if this was the case, we would expect to see some evidence of a peak in the results. Finally, diffusion rates may have decreased at higher L, which once again may be related to the 2+ days of quiet conditions. Again, these results are consistent with the results of *Onsager et al.* [2004], who found the gradient near GEO to be positive during quiet conditions.

[31] We find 48 mixed gradient events in this study, which is indicative of two distinct populations. Of these, there are 41 in which the PSD gradient is negative for 2000 MeV/G electrons, while being positive or flat for 50 MeV/G electrons. This is consistent with the expected results of the theory of relativistic electron heating by wave-particle interactions. By this theory, electrons with energy greater than a couple hundred keV have a source somewhere outside of the plasmapause [*Meredith et al.*, 2001; 2003] where local heating by whistler mode chorus [e.g., *Horne and Thorne*, 1998; *Summers et al.*, 1998] and/or magnetosonic waves [e.g., *Horne et al.*, 2007] occurs, and lower-energy electrons (energy of tens of keV to a couple hundred keV) have a source at higher L^* due to substorm injections and convection [e.g., *Meredith et al.*, 2003 and references therein]. The timescales for relativistic electron heating by wave-particle interactions are about the same for both whistler mode chorus and magnetosonic waves, around 1–2 days [*Horne et al.*, 2005; *Horne et al.*, 2007], and both whistler mode chorus and magnetosonic waves tend to be more intense with enhanced AE^*, which indicates a connection between these waves and substorm activity and/or periods of enhanced convection [*Meredith et al.*, 2001; 2008]. Finally, *Bortnik and Thorne* [2007] defined an "anchor point" energy of a couple of hundred keV at which electrons with greater energy tend to be accelerated by interactions with whistler mode chorus, while those with less energy tend to be scattered and lost by the interactions.

[32] This is all consistent with the majority of the mixed gradient event results in that the gradient of electrons with μ greater than a couple hundred MeV per Gauss (equivalent to those with energy above a couple hundred keV at GEO) is negative beyond GEO, which may be the result of a PSD source inside of GEO prior to the event time. Meanwhile, for these same events, the gradient of electrons with μ less than a couple hundred MeV per Gauss is positive or relatively flat, indicating a source outside of GEO, and electrons with μ between around 100 and 300 MeV/G consistently mark the transition region between the two populations. Also, based on the example mixed gradient event and the superposed epoch analysis results, the *AE* and AE^* indexes are typically high in the days leading up to those events that reveal a negative gradient for 2000 MeV/G electrons. Last, it is stressed that the opposite situation, in which the gradient of 2000 MeV/G electrons is either positive or flat while the gradient of 50 MeV/G electrons is negative, is not observed.

6.3. Discussion of the Superposed Epoch Analysis

[33] The most significant features of the superposed epoch analysis are the differences in IMF B_z, *Kp*, *AE*, AE^*, and fluxes at different energies, as well as the vastly different conditions at greater than ~50 h that can produce all-positive PSD gradient results. The *AE* and AE^* indexes are consistently high, on average, for the negative gradient events, and

there is considerable activity in both indexes during the active periods preceding two of the positive gradient events. However, after −48 h ET, the *AE* and *AE** levels drop significantly for the positive gradient events, while remaining high for the negative gradient events. On this, *Meredith et al.* [2003] reported that the most significant electron enhancements, which they also relate to chorus-driven acceleration, are associated with prolonged substorm activity, where the *AE* index is greater than 100 nT for a total integrated time of more than two days. The *AE* index is, on average, around 200 nT for more than two days leading up to the negative gradient events, whereas for the positive gradient events, it drops to below 100 nT and remains almost consistently below this level in the two days leading up to the events. Finally, the differences in the two sets of fluxes prior to the events (see Figure 10) are also consistent with the results of *Meredith et al.* [2003], who found that significant flux enhancements are also associated with enhanced fluxes of electrons at a couple hundred keV.

[34] We believe that the weak statistics of the four all-positive gradient events provide further insight into an important time scale for the outer-belt electrons. First of all, the active periods are only seen at greater than 50 h for two of the four events, but all four events are classified as that in which the PSD gradients over the full range of μ is positive beyond GEO. Thus, either both active conditions and quiet conditions over five days can lead to positive PSD gradients beyond GEO or what happens more than two days before the event is not as important as what happens in the two days leading up to it. Based on previous studies, positive gradients beyond GEO have been observed during quiet times [e.g., *Onsager et al.*, 2004 and references therein], but during active conditions, particularly, geomagnetic storms, negative gradients have been observed beyond GEO for high-energy electrons [e.g., *Chen et al.*, 2007a]. Taking these previous results into account with our own, we propose that the outer-belt electrons may have an effective "memory" of approximately two days.

7. Conclusions and Further Work

[35] Here, we have studied the radial gradients of outer-belt electron PSD prior to 86 sudden solar wind pressure enhancement events. Of these, the majority reveal that the gradient for electrons with μ = 2000 MeV/G is negative, which is consistent with the results of *Chen et al.* [2007b], while the gradient for electrons with μ = 50 MeV/G is positive or relatively flat, and there is a transition between the two types of gradient normally for electrons with μ around 200 MeV/G. This is indicative of two different source populations for near-equatorially mirroring electrons with high and low energies. We have discussed how the results for 41 of the 86 cases can be explained directly by the current theory and understanding of relativistic electron acceleration by wave-particle interactions. Additionally, we have examined the preconditions for several examples of distinct types of PSD gradient results. One of the most notable features of these different examples is the geomagnetic activity in the 0–2 days leading up to the event times; the events in which a negative gradient is seen for 2000 MeV/G electrons have considerably higher *Kp* and *AE* levels than those for the events in which a positive gradient is seen for 2000 MeV/G electrons. A superposed epoch analysis has also been conducted, and it reveals similar differences.

[36] Results here indicate that 1–2 days is a significantly important timescale to the outer-belt electrons, though this should not come as a surprise as other studies have repeatedly found this to be true [e.g., *Baker et al.*, 1994; *Horne et al.*, 2003; 2007; *Li et al.*, 2005; *Burin des Roziers et al.*, 2009]. Events that show at least two days of little to no geomagnetic activity tend to produce positive or flat gradients over the full range of μ's examined, whereas geomagnetic activity (evident in the *AE* and *Kp* indexes) in the 0–2 days prior to events tends to produce negative gradients for the higher-energy electrons. This is indicative of the great importance of substorms and/or enhanced convection to the gradient results, and thus, outer-belt electron acceleration. This is consistent with the findings of *Li et al.* [1998] and *Meredith et al.* [2002; 2003], and is also additional evidence that approximately two days is an important timescale for the outer-belt electrons.

[37] It is important to note that these conclusions are consistent with those of previous studies, though they are independent and come from the results of a new analysis technique. This study provides new observational evidence agreeing with the combined works of several, independent studies on the acceleration of outer-belt electrons by wave-particle interactions. Also, the results presented here extend our understanding of outer radiation belt dynamics and provide a broad context for comparisons with previous PSD gradient studies since this study examines PSD gradients resulting from quiet, moderate, and active geomagnetic conditions for outer-belt electrons at and beyond GEO over a very broad range of energies (tens of keV to >1 MeV).

[38] This paper introduces a great deal of additional studies that can be conducted. Test-particle simulations can be used for selected individual events to determine how far electrons are transported radially inward and to quantify the gradient. Also, the analysis technique can be applied to spacecraft measurements made in orbits outside of GEO. This study does not include ULF wave power, which would be interesting to analyze for these events in an attempt to establish any correlation with the different PSD gradients, since it has been established that ULF waves are critical to enhanced radial diffusion [e.g., *Elkington et al.*, 1999] and previous studies find that they may be important to electron acceleration beyond GEO [e.g., *O'Brien et al.*, 2003]. Finally, considering the apparent importance of substorm activity to how outer-belt electron radial gradients develop, a survey of relativistic electron responses to substorms, similar to either of those conducted for geomagnetic storms by *O'Brien et al.* [2001] or *Reeves et al.* [2003], should prove to be beneficial to the community.

[39] Many questions remain concerning Earth's outer-belt electrons, and as we become more dependent on satellites in this region of space, better understanding and models of the outer radiation belt become increasingly more important. As more evidence of local heating by wave-particle interactions is discovered, the question of electron acceleration appears to be getting clearer. However, the events examined for this study still display some of the complexity in the nature of the outer radiation belt electrons. Hopefully, future missions like NASA's Radiation Belt Storm Probes will provide the

measurements needed to further resolve some of the outstanding issues.

[40] **Acknowledgments.** We would like to thank James McCollough, Weichao Tu, and Edward Burin des Roziers for useful insight and discussions. We are also very grateful to the World Data Center for Geomagnetism, Kyoto, Japan, the Coordinated Data Analysis Web (CDAWeb), and the LANL energetic particles team for their online data access. This work was supported by NSF grants (ATM-0549093 and ATM-0902813) and also by grants from the National Natural Science Foundation of China (40621003 and 40728005).

[41] Zuyin Pu thanks the reviewers for their assistance in evaluating this paper.

References

Baker, D. N., J. B. Blake, L. B. Callis, J. R. Cummings, D. Hovestadt, S. G. Kanekal, B. Klecker, R. A. Mewaldt, and R. D. Zwickl (1994), Relativistic electron acceleration and decay times in the inner and outer radiation belts: SAMPEX, *Geophys. Res. Lett.*, *21*, 409–412, doi:10.1029/93GL03532.

Bortnik, J., and R. M. Thorne (2007), The dual role of ELF/VLF chorus waves in the acceleration and precipitation of radiation belt electrons, *J. Atmos. Sol. Terr. Phys.*, *69*, 378–386, doi:10.1016/j.jastp.2006.05.030.

Brautigam, D. H., and J. M. Albert (2000), Radial diffusion analysis of outer radiation belt electrons during the October 9, 1990, magnetic storm, *J. Geophys. Res.*, *105*, 291–309, doi:10.1029/1999JA900344.

Burin des Roziers, E., X. Li, D. N. Baker, T. A. Fritz, R. Friedel, T. G. Onsager, and I. Dandouras (2009), Energetic plasma sheet electrons and their relationship with the solar wind: A Cluster and Geotail study, *J. Geophys. Res.*, *114*, A02220, doi:10.1029/2008JA013696.

Carpenter, D. L., and R. R. Anderson (1992), An ISEE/whistler model of equatorial electron density in the magnetosphere, *J. Geophys. Res.*, *97*, 1097–1108, doi:10.1029/91JA01548.

Chen, Y., R. H. W. Friedel, G. D. Reeves, T. G. Onsager, and M. F. Thomsen (2005), Multisatellite determination of the relativistic electron phase space density at geosynchronous orbit: Methodology and results during geomagnetically quiet times, *J. Geophys. Res.*, *110*, A10210, doi:10.1029/2004JA010895.

Chen, Y., R. H. W. Friedel, and G. D. Reeves (2006), Phase space density distributions of energetic electrons in the outer radiation belt during two Geospace Environment Modeling Inner Magnetosphere/Storms selected storms, *J. Geophys. Res.*, *111*, A11S04, doi:10.1029/2006JA011703.

Chen, Y., R. H. W. Friedel, G. D. Reeves, T. E. Cayton, and R. Christensen (2007a), Multisatellite determination of the relativistic electron phase space density at geosynchronous orbit: An integrated investigation during geomagnetic storm times, *J. Geophys. Res.*, *112*, A11214, doi:10.1029/2007JA012314.

Chen, Y., G. D. Reeves, and R. H. W. Freidel (2007b), The energization of relativistic electrons in the outer Van Allen radiation belt, *Nat. Phys.*, *3*, 614–617, doi:10.1038/nphys655.

Elkington, S. R., M. K. Hudson, and A. A. Chan (1999), Acceleration of relativistic electrons via drift-resonant interaction with toroidal-mode Pc-5 ULF oscillation, *Geophys. Res. Lett.*, *26*, 3273–3276, doi:10.1029/1999GL003659.

Friedel, R. H. W., G. D. Reeves, and T. Obara (2002), Relativistic electron dynamics in the inner magnetosphere: A review, *J. Atmos. Sol. Terr. Phys.*, *64*, 265–282, doi:10.1016/S1364-6826(01)00088-8.

Green, J. C., and M. G. Kivelson (2004), Relativistic electrons in the outer radiation belt: Differentiating between acceleration mechanisms, *J. Geophys. Res.*, *109*, A03213, doi:10.1029/2003JA010153.

Hilmer, R. V., G. P. Ginet, and T. E. Cayton (2000), Enhancement of equatorial energetic electron fluxes near $L = 4.2$ as a result of high speed solar wind streams, *J. Geophys. Res.*, *105*, 23,111–23,322, doi:10.1029/1999JA000380.

Horne, R. B., and R. M. Thorne (1998), Potential waves for relativistic electron scattering and stochastic acceleration during magnetic storms, *Geophys. Res. Lett.*, *25*, 3011–3014, doi:10.1029/98GL01002.

Horne, R. B., S. A. Glauert, and R. M. Thorne (2003), Resonant diffusion of radiation belt electrons by whistler-mode chorus, *Geophys. Res. Lett.*, *30*(9), 1493, doi:10.1029/2003GL016963.

Horne, R. B., R. M. Thorne, S. A. Glauert, J. M. Albert, N. P. Meredith, and R. R. Anderson (2005), Timescale for radiation belt electron acceleration by whistler mode chorus waves, *J. Geophys. Res.*, *110*, A03225, doi:10.1029/2004JA010811.

Horne, R. B., R. M. Thorne, S. A. Glauert, N. P. Meredith, D. Pokhotelov, and O. Santolík (2007), Electron acceleration in the Van Allen radiation belts by fast magnetosonic waves, *Geophys. Res. Lett.*, *34*, L17107, doi:10.1029/2007GL030267.

Iles, R. H. A., N. P. Meredith, A. N. Fazakerley, and R. B. Horne (2006), Phase space density analysis of the outer radiation belt energetic electron dynamics, *J. Geophys. Res.*, *111*, A03204, doi:10.1029/2005JA011206.

Ingraham, J. C., T. E. Cayton, R. D. Belian, R. A. Christensen, R. H. W. Friedel, M. M. Meier, G. D. Reeves, and M. Tuszewski (2001), Substorm injection of relativistic electrons to geosynchronous orbit during the great magnetic storm of March 24, 1991, *J. Geophys. Res.*, *106*, 25,759–25,776, doi:10.1029/2000JA000458.

Lee, D.-Y., L. R. Lyons, and G. D. Reeves (2005), Comparison of geosynchronous energetic particle flux responses to solar wind dynamic pressure enhancements and substorms, *J. Geophys. Res.*, *110*, A09213, doi:10.1029/2005JA011091.

Li, X., I. Roth, M. Temerin, J. Wygant, M. K. Hudson, and J. B. Blake (1993), Simulation of the prompt energization and transport of radiation belt particles during the March 23, 1991 SSC, *Geophys. Res. Lett.*, *20*, 2423–2426, doi:10.1029/93GL02701.

Li, X., D. N. Baker, M. Temerin, G. Reeves, and R. Belian (1998), Simulation of dispersionless injections and drift echoes of energetic electrons associated with substorms, *Geophys. Res. Lett.*, *25*, 3763–3766, doi:10.1029/1998GL900001.

Li, X., D. N. Baker, M. Temerin, T. E. Cayton, G. D. Reeves, R. S. Selesnick, J. B. Blake, G. Lu, S. G. Kanekal, and H. J. Singer (1999), Rapid enhancements of relativistic electrons deep in the magnetosphere during the May 15, 1997, magnetic storm, *J. Geophys. Res.*, *104*, 4467–4476, doi:10.1029/1998JA900092.

Li, X., D. N. Baker, S. Elkington, M. Temerin, G. D. Reeves, R. D. Belian, J. B. Blake, H. J. Singer, W. Peria, and G. Parks (2003), Energetic particle injections in the inner magnetosphere as a response to an interplanetary shock, *J. Atmos. Sol. Terr. Phys.*, *65*, 233–244, doi:10.1016/S1364-6826(02)00286-9.

Li, X., D. N. Baker, M. Temerin, G. D. Reeves, R. Friedel, and C. Shen (2005), Energetic electrons, 50 keV–6 MeV, at geosynchronous orbit: Their responses to solar wind variations, *Space Weather*, *3*, S04001, doi:10.1029/2004SW000105.

McAdams, K. L., G. D. Reeves, R. H. W. Friedel, and T. E. Cayton (2001), Multi-satellite comparisons of the radiation belt response to the GEM magnetic storms, *J. Geophys. Res.*, *106*, 10,869–10,882, doi:10.1029/2000JA000248.

McGuire, R. E., R. J. Burley, R. M. Candey, R. L. Kessel, and T. J. Kovalick (2000), CDAWeb and SSCWeb: Enabling correlative international Sun-Earth-connections science entering the era of IMAGE and Cluster, *Eos Trans. AGU*, *81*(19), Spring Meet. Suppl., Abstract SM32A-14.

Meredith, N. P., R. B. Horne, and R. R. Anderson (2001), Substorm dependence of chorus amplitudes: Implications for the acceleration of electrons to relativistic energies, *J. Geophys. Res.*, *106*, 13,165–13,178, doi:10.1029/2000JA900156.

Meredith, N. P., R. B. Horne, R. H. A. Iles, R. M. Thorne, D. Heynderikx, and R. R. Anderson (2002), Outer zone relativistic electron acceleration associated with substorm-enhanced whistler mode chorus, *J. Geophys. Res.*, *107*(A7), 1144, doi:10.1029/2001JA900146.

Meredith, N. P., M. Cain, R. B. Horne, R. M. Thorne, D. Summers, and R. R. Anderson (2003), Evidence for chorus-driven electron acceleration to relativistic energies from a survey of geomagnetically disturbed periods, *J. Geophys. Res.*, *108*(A6), 1248, doi:10.1029/2002JA009764.

Meredith, N. P., R. B. Horne, and R. R. Anderson (2008), Survey of magnetosonic waves and proton ring distributions in the Earth's inner magnetosphere, *J. Geophys. Res.*, *113*, A06213, doi:10.1029/2007JA012975.

O'Brien, T. P., and M. B. Moldwin (2003), Empirical plasma pause models from magnetic indices, *Geophys. Res. Lett.*, *30*(4), 1152, doi:10.1029/2002GL016007.

O'Brien, T. P., R. L. McPherron, D. Sornette, G. D. Reeves, R. Friedel, and H. J. Singer (2001), Which magnetic storms produce relativistic electrons at geosynchronous orbit?, *J. Geophys. Res.*, *106*, 15,533–15,544, doi:10.1029/2001JA000052.

O'Brien, T. P., K. R. Lorentzen, I. R. Mann, N. P. Meredith, J. B. Blake, J. F. Fennell, M. D. Looper, D. K. Milling, and R. R. Anderson (2003), Energization of relativistic electrons in the presence of ULF power and MeV microbursts: Evidence for dual ULF and VLF acceleration, *J. Geophys. Res.*, *108*(A8), 1329, doi:10.1029/2002JA009784.

Onsager, T. G., A. A. Chan, Y. Fei, S. R. Elkington, J. C. Green, and H. J. Singer (2004), The radial gradient of relativistic electrons at geosynchronous orbit, *J. Geophys. Res.*, *109*, A05221, doi:10.1029/2003JA010368.

Petrinec, S. M., and C. T. Russell (1996), Near-Earth magnetotail shape and size as determined from the magnetopause flaring angle, *J. Geophys. Res.*, *101*, 137–152, doi:10.1029/95JA02834.

Reeves, G. D., D. N. Baker, R. D. Belian, J. B. Blake, T. E. Cayton, J. F. Fennel, R. H. W. Friedel, M. M. Meier, R. S. Selesnick, and H. E. Spence (1998), The global response of relativistic radiation belt elec-

trons to the January 1997 magnetic cloud, *Geophys. Res. Lett.*, *17*, 3265–3268, doi:10.1029/98GL02509.

Reeves, G. D., K. L. McAdams, R. H. W. Friedel, and T. P. O'Brien (2003), Acceleration and loss of relativistic electrons during geomagnetic storms, *Geophys. Res. Lett.*, *30*(10), 1529, doi:10.1029/2002GL016513.

Roederer, J. G. (1970), *Dynamics of Geomagnetically Trapped Radiation*, Springer, Berlin.

Schulz, M., and L. Lanzerotti (1974), *Particle Diffusion in the Radiation Belts*, Springer, New York.

Selesnick, R. S., and J. B. Blake (2000), On the source location of radiation belt relativistic electrons, *J. Geophys. Res.*, *105*, 2607–2624, doi:10.1029/1999JA900445.

Selesnick, R. S., J. B. Blake, W. A. Kolasinski, and T. A. Fritz (1997), A quiescent state of 3 to 8 MeV radiation belt electrons, *Geophys. Res. Lett.*, *24*, 1343–1346, doi:10.1029/97GL51407.

Shi, Y., E. Zesta, and L. R. Lyons (2009), Features of energetic particle radial profiles inferred from geosynchronous responses to solar wind dynamic pressure enhancements, *Ann. Geophys.*, *27*, 851–859.

Summers, D., R. M. Thorne, and F. Xiao (1998), Relativistic theory of wave-particle resonant diffusion with application to electron acceleration in the magnetosphere, *J. Geophys. Res.*, *103*, 20,487–20,500, doi:10.1029/98JA01740.

Taylor, M. G. G. T., R. H. W. Friedel, G. D. Reeves, M. W. Dunlop, T. A. Fritz, P. W. Daly, and A. Balogh (2004), Multisatellite measurements of electron phase space density gradients in the Earth's inner and outer magnetosphere, *J. Geophys. Res.*, *109*, A05220, doi:10.1029/2003JA010294.

Temerin, M., I. Roth, M. K. Hudson, and J. R. Wygant (1994), New paradigm for the transport and energization of radiation belt particles, *Eos Trans. AGU*, *75*(44), *Fall Meet.*, Suppl., 538.

Tu, W., X. Li, Y. Chen, G. D. Reeves, and M. Temerin (2009), Storm-dependent radiation belt electron dynamics, *J. Geophys. Res.*, *114*, A02217, doi:10.1029/2008JA013480.

Turner, D. L., and X. Li (2008), Radial gradients of phase space density of the outer radiation belt electrons prior to sudden solar wind pressure enhancements, *Geophys. Res. Lett.*, *35*, L18101, doi:10.1029/2008GL034866.

X. Li and D. L. Turner, Laboratory for Atmospheric and Space Physics, University of Colorado at Boulder, 1234 Innovation Dr., Boulder, CO 80303, USA. (drew.lawson.turner@gmail.com)

G. D. Reeves, Space and Atmospheric Sciences Group, Los Alamos National Laboratory, NIS-1, MS D-466, Los Alamos, NM 87545, USA.

H. J. Singer, Space Weather Prediction Center, National Oceanic and Atmospheric Administration, 325 Broadway, Boulder, CO 80305, USA.